Coplanar electrowetting-induced stirring as a tool to manipulate biological samples in lubricated digital microfluidics. Impact of ambient phase on drop internal flow pattern[a)]

Laurent Davoust,[1,b)] Yves Fouillet,[2] Rachid Malk,[2] and Johannes Theisen[3]
[1]*Grenoble Institute of Technology (Grenoble-INP), Materials and Processes Science and Engineering Laboratory (SIMAP), BP 75, 38402 Saint Martin d'Hères, France*
[2]*CEA-LETI-MINATEC, 38041 Grenoble cedex 9, France*
[3]*University of Grenoble (UJF), Laboratory of Geophysical and Industrial Fluid Flows (LEGI), BP 53, 38041 Grenoble, France*

(Received 28 April 2013; accepted 17 July 2013; published online 25 July 2013)

Oscillating electrowetting on dielectrics (EWOD) with coplanar electrodes is investigated in this paper as a way to provide efficient stirring within a drop with biological content. A supporting model inspired from Ko *et al.* [Appl. Phys. Lett. **94**, 194102 (2009)] is proposed allowing to interpret oscillating EWOD-induced drop internal flow as the result of a current streaming along the drop surface deformed by capillary waves. Current streaming behaves essentially as a surface flow generator and the momentum it sustains within the (viscous) drop is even more significant as the surface to volume ratio is small. With the circular electrode pair considered in this paper, oscillating EWOD sustains toroidal vortical flows when the experiments are conducted with aqueous drops in air as ambient phase. But when oil is used as ambient phase, it is demonstrated that the presence of an electrode gap is responsible for a change in drop shape: a pinch-off at the electrode gap yields a peanut-shaped drop and a symmetry break-up of the EWOD-induced flow pattern. Viscosity of oil is also responsible for promoting an efficient damping of the capillary waves which populate the surface of the actuated drop. As a result, the capillary network switches from one standing wave to two superimposed traveling waves of different mechanical energy, provided that actuation frequency is large enough, for instance, as large as the one commonly used in electrowetting applications ($f \sim 500$ Hz and beyond). Special emphasis is put on stirring of biological samples. As a typical application, it is demonstrated how beads or cell clusters can be focused under flow either at mid-height of the drop or near the wetting plane, depending on how the nature of the capillary waves is (standing or traveling), and therefore, depending on the actuation frequency (150 Hz–1 KHz).
 [http://dx.doi.org/10.1063/1.4817006]

I. INTRODUCTION

Overcoming diffusion of molecules and mixing of reagents in biotechnological applications and assays is challenging, the aim being to ensure rapid and efficient assays.[2] New ways of realizing stirring in miniaturized systems like lab-on-chips are worthy to be explored. A second application of large importance at the scale of micro-systems is the preparation of biological samples with the purpose to extract biologically functionalized beads or clusters of cells, for instance.

As a technological breakthrough, ElectroWetting On Dielectric (EWOD) stands as a new driving mechanism in micro-systems like variable focal lenses,[3] displays[4] or digital lab-on-a-chip devices for

[a)]Paper submitted as part of the 3rd European Conference on Microfluidics (Guest Editors: J. Brandner, S. Colin, G. L. Morini). The Conference was held in Heidelberg, Germany, December 3–5, 2012.
[b)]Author to whom correspondence should be addressed. Electronic mail: laurent.davoust@simap.grenoble-inp.fr.

clinical diagnostics[5] or biological environmental monitoring.[6] Used in AC mode at a frequency, f ∼ 1 KHz or more, EWOD is used as a common means to move, merge or break-up drops.[7] EWOD can also be used at a lower frequency in a regime referred to as oscillating EWOD (f ∼ 100 Hz). This permits to induce shape oscillations of a sessile drop which in return generates a Stokes drift along its liquid surface. Subsequently, oscillating EWOD has been proposed as a mixing promoter in two popular configurations of electrowetting: the parallel-plate[7,8] and needle[9–12] configurations.

In this paper, oscillating EWOD-induced drop stirring is provided with a coplanar electrode open configuration which reveals itself to be easily integrable into state-of-the-art digital lab-on-chips. As a consequence, EWOD-induced mixing enhancement is experimentally promoted without the presence of a plunging needle as a counter-electrode.

In presence of a needle, the electrostatic map is changed compared to the one of the coplanar configuration,[13] at least for a large enough frequency (f ∼ 10–100 KHz), and capillary effects due to moving meniscus along the needle should be taken into account.

Coplanar geometry allows us to compare in best conditions our experimental results with current streaming theory available in the literature either at bubble scale,[1] or at the scale of a droplet in air as ambient phase[10] or, eventually at the scale of a droplet in oil as ambient phase (see Ko *et al.*[14] for the moment but coupling with electrostatics is not considered). Typically, when the frequency is small enough and the ambient phase is air, coplanar EWOD results in a single spherical standing wave along the drop surface with capillary resonance[15] properly achieved at the apex.[16,17]

In a first part of this paper, it is demonstrated how EWOD-induced stirring can be considered as a liquid surface flow generator; the surface momentum it generates is dissipated within the viscous drop; the smaller the drop is, the more efficient this surface flow generator is.

A second part is devoted to a symmetry break-up of the internal flow pattern, jointly induced by the presence of an electrode gap and the use of oil as alternative ambient phase.

A last part is devoted to biological applications of oscillating EWOD used to focus colloidal beads and biological cells (U373B) at drop scale.

II. MATERIALS AND METHODS

Technological steps are performed on a 200 mm silicon wafer and EWOD chips are composed of three main layers: the electrodes (200 nm thick AlCu); the dielectric layer (600 nm thick Si3N4); and, finally, the hydrophobic layer (1 μm thick SiOC). These materials enable to integrate the whole fabrication process into cleanrooms with no compromise on EWOD performance and a good reproducibility during assays. More details of the technology are given in Malk *et al.*[18]

The chip design used here consists of two half disks shaped coplanar electrodes (radius = 2 mm) separated by a 3 μm-gap (as regards experiments with air as ambient phase) or a 100 μm-gap (as regards experiments with oil as ambient phase, Figs. 1 and 2). A first advantage of this coplanar electrode configuration—compared with the classic needle electrode configuration—is that droplet deformation is not disturbed by meniscus effect due to the presence of a needle electrode. Consequently, top views with image analysis are made possible. A second advantage lies on the circular geometry of the two facing electrodes which enhances isotropic electrowetting of the sessile drop and makes analytical modeling possible.

AC electric signal is generated from a generator (Yokogawa FG120) and a home-made amplifier. A CCD camera (Pixelfly 200 XS) and a zoom lens are used for image acquisition. The camera is placed so as to visualize droplet profiles (Fig. 2). A LED is used as a stroboscopic lighting source placed behind the droplet in order to create a backlight and to minimize light reflection. The LED is plugged to the same generator. The frequencies of AC actuation and stroboscopic lighting are equal, and by shifting the phase lag between both signals, the instantaneous shape of the droplet can be clearly imaged. Time-dependent droplet profiles are thus acquired and analyzed using home-made software.

Drop convective flow is simultaneously analyzed by imaging fluorescent beads (mean diameter: 10 μm and mean density: 1.05) and using a software dedicated to micro-PIV (Particle

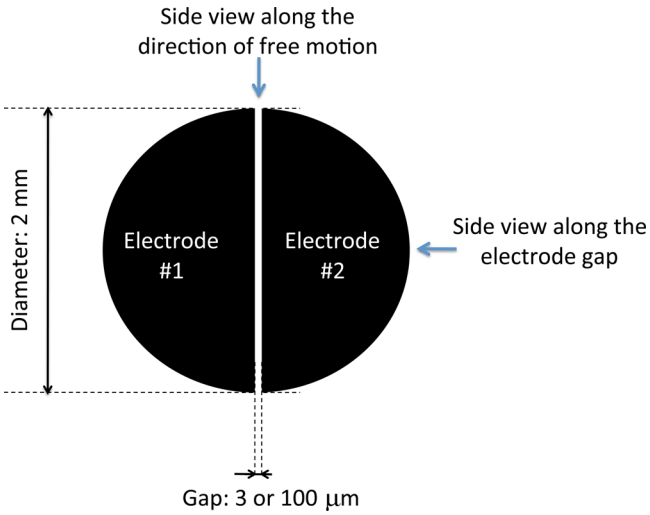

FIG. 1. Design of the electrode pair under consideration.

Image Velocimetry). The laser sheet used to induce bead fluorescence is provided by a laser source (Melles Griot: 5mW, $\lambda = 470$ nm) and a series of two cylindrical lenses (thickness of laser sheet at drop position: 100 μm). A 532 nm filter is fitted to the zoom lens to detect fluorescence. It is thus possible to characterize simultaneously both the flow and the droplet oscillations at different frequencies of the applied voltage. With the beads and the lighting source used in the experiments, the flow that is observed is the drop surface flow. For the observation of internal flows, use is made of the laser sheet.

Most of the experiments are realized with a 1.5 μl drop of Phosphate Buffered Saline (PBS) deposited on the lubricated chip surface with a micropipette. Depending on the experiments, air or silicone oil (RT5, Paragon Scientific, dynamical viscosity: $\mu = 4{,}9$ mPa s) can be

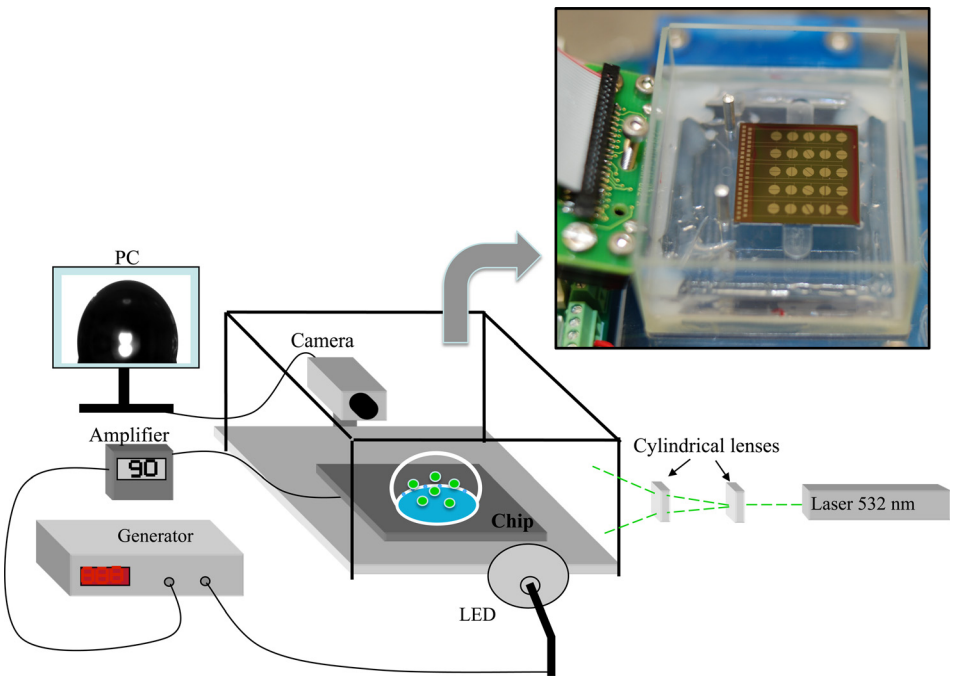

FIG. 2. Experimental setup and array of EWOD chips in the upper frame.

TABLE I. Wetting data in static conditions with the EWOD chip considered in this study.

	PBS drop in:	Air	Oil
None EWOD	Surface tension (N/m)	72	28
None EWOD	Contact angle	107°	158○
None EWOD	Contact angle hysteresis	5° − 7°	<3° (∼ goniometer resolution)
EWOD (no saturation)	Contact angle at 90 V rms	91°	124°

used as ambient phase. Surface tensions, contact angles and capillary hysteresis as directly measured along the surface of coplanar chips with a goniometer (Kruss, DSA 100), are given in Table I.

Experiments with oil as ambient phase have been realized on drops populated by three types of cells commonly used in biology or medical assays: red blood cells, white blood cells and U373B cells. Their characteristics are detailed in Table II.

Because of their transparency, white blood cells were labeled with a fluorescent tag to facilitate imaging. As regards U373B cells, they have been selected because they are extensively cultivated in the laboratory[19] and because, unlike red blood cells, the U373B cells tend to stick to solid surfaces. They are solubilized in a dedicated culture medium containing 10% of fetal calf serum.

III. OSCILLATING EWOD-INDUCED STREAMING FLOW IN AIR AS AMBIENT PHASE (ISOTROPIC WETTING)

Half-circular coplanar electrodes under consideration here are separated by a gap as small as possible, 3 μm, which is expected to be particularly in favor with isotropic electrowetting of a drop. When use is made of air as ambient phase, stirring is found to remain perfectly 2-D axisymmetric, with the arising of superimposed toroidal vortices, provided that the frequency of the electric actuation remains under the critical onset of 450 Hz. As confirmed in the following, the even number of toroidal vortices is directly driven by a resonant eigenmode of a capillary standing wave along the drop surface. In fact, a traveling capillary wave (TCW) is excited from the contact line which moves back and forth under the oscillating electric stress. This wave propagates radially inwards up to the apex where a wave interaction is expected to occur. As a result, a second TCW is excited by the vertically moving apex, which travels radially outwards down to the contact line.[15,20] In steady conditions, a resonance mechanism between these two TCW is therefore expected: drop deformation is observed to be the largest at the drop apex and the contact line, which behave as the antinodes of a resulting standing capillary wave.

A. Analysis of vortex position versus frequency

The vortices located within a meridian plane of the droplet are steady and, interestingly, when increasing the actuation frequency, their number increases while being always even. Our experiments demonstrate a surprising reproducibility and reversibility of the vortex locations and number when actuation frequency ranges from 450 Hz to 150 Hz and vice versa. The

TABLE II. Characteristics of the biological cells.

	Red blood cells	White blood cells	U373B cells
Size	2–8 μm	10–30 μm	20–40 μm
Shape	Disk	Sphere	Sphere, adhesive cells
Concentration (cells/μl)	5.5×10^3	$0.5 \times 10^3 - 1 \times 10^3$	1.5×10^3
Liquid medium	PBS	PBS	Culture medium

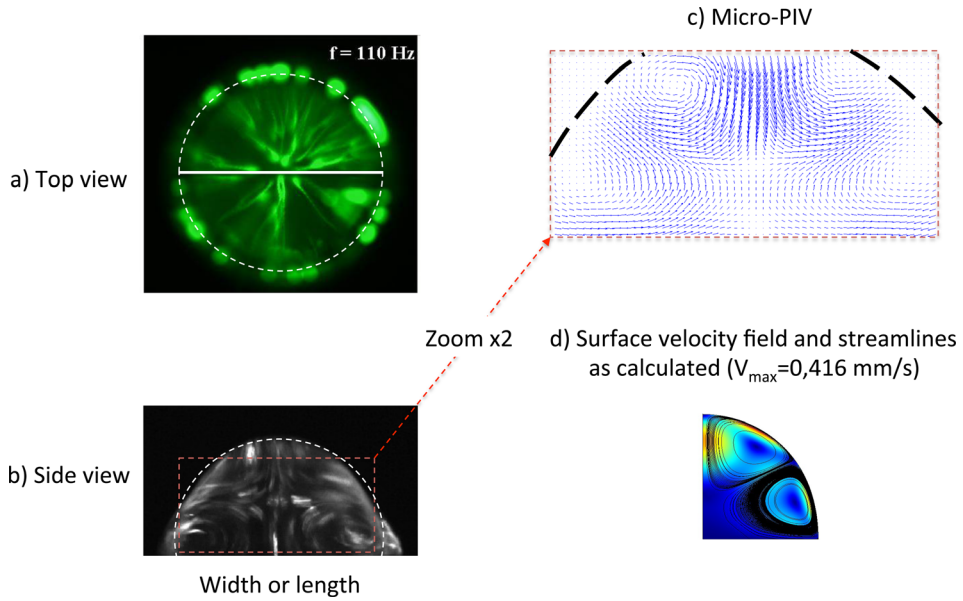

FIG. 3. Axisymmetric flow within a sessile PBS drop in air, under oscillating EWOD as observed from (a) above with fluorescent tracers, (b) along a drop cross-section (use of a 100 μm thick laser sheet, the white dotted contour indicates the averaged half-spherical drop shape), and (c) experimental velocity field as obtained from micro-PIV along a meridian cross-section; arrows emphasize the presence of the toroidal counterrotating vortex pair. For the sake of comparison, (d) toroidal vortices as calculated along a meridian cross-section. Chip with two half-circular electrodes separated by a gap of 3 μm, actuation frequency: f = 110 Hz, RMS voltage: 60 V, wave number: k = 2.

droplet oscillations induced by AC EWOD are also simultaneously observed by switching from laser lighting to stroboscopic lighting.[21] Any change in the input frequency also yields a change in the oscillation mode. In Fig. 3, top view (a) and side view (b) of the flow are displayed for an input frequency, f = 110 Hz, with the arising of two permanent toroidal structures.

At 110 Hz, the amplitude of drop shape oscillations is found maximum at the apex and at mid-height of the droplet, which corresponds to the second radial eigenmode (k = 2), see, e.g., Kang *et al.*[22] Clearly, the vortices and subsequent drop stirring flow are induced by the capillary standing wave excited along the drop surface from the actuated oscillating contact line.

It is also worthy to notice that due to the slow timescale of the viscous diffusion of momentum, stirring flow is more and more confined near the drop surface when the actuation frequency increases.

B. EWOD-induced streaming current as a surface flow generator

For a frequency $f = \frac{\omega_k}{2\pi}$ of the AC voltage, the drop oscillates with a frequency $f_g = \frac{\xi_k}{2\pi} = \frac{\omega_k}{\pi}$ since the electric stress upon the contact line scales as the square of the applied voltage. The shape of the oscillating drop can be fairly described as a half-sphere modulated by a radial deformation,

$$r = R_0 + A_k \sin(\xi_k t + \psi_k) P_k(\cos(\theta)),$$

where θ is the colatitude, A_k is the amplitude of drop oscillations for the eigenmode, k, ξ_k is the angular frequency, ψ_k is the associated phase lag, P_k is kth-degree Legendre polynomial, and R_0 is the averaged radius of the sessile drop which behaves as a non-deformed half-sphere when the voltage frequency is large enough (>1 KHz): $R_o = (\frac{3V_l}{2\pi})^{\frac{1}{3}}$, with V_l, the liquid volume deposited.

For a standing wavy surface deformed with a kth-eigenmode, the time-dependent velocity potential in the inner of the drop writes as:[23,24]

$$\Phi_i = -\frac{A_k \xi_k R_o}{k} \frac{r^k}{R_o^k} P_k(\cos(\theta))\cos(\xi_k t + \psi_k).$$

Hence, it is possible to calculate the normal component of the surface velocity, $u_k^\infty = -\frac{1}{R_o}\frac{\partial \Phi_i}{\partial \theta}\big|_{r=R_o}$, as follows:

$$u_k^\infty = U_k^\infty \cos(\xi_k t + \psi_k),$$

where

$$U_k^\infty = \frac{A_k \xi_k}{k} P_k(\cos(\theta)),$$

is nothing but the normal velocity of the standing wave. Considering a Strouhal number large enough,

$$S = \frac{\xi_k R_o}{U_k^\infty} \gg 1,$$

and therefore, the theory of steady streaming,[25,26] it is demonstrated, in a way similar to Ko *et al.* for electrowetting-driven bubble oscillations,[1] that a steady component of the velocity, $U_k{}^s$, referred to as streaming current, is provided at the boundary of (and beyond) a Stokes layer staying along the inner of the moving drop surface and writes as:

$$U_k^s = -\frac{3}{8R_0\xi_k}\frac{d}{d\theta}[(U_k^\infty)^2],$$

or in terms of Legendre polynomials:

$$U_k^s = -\frac{3A_k^2\xi_k}{8R_0k^2}\frac{d}{d\theta}\left[\left(\frac{dP_k(\cos\theta)}{d\theta}\right)^2\right]. \quad (1)$$

In our case, the thickness of the Stokes layer is much thinner than the drop radius, $\delta_s = \mathcal{O}(\sqrt{\frac{\eta}{\rho\xi_k}}) \ll R_o$, with η and ρ, the viscosity and the density of the drop, respectively (Table III). And consequently, the streaming velocity can be considered as a surface boundary condition for the drop convective flow, which therefore may be calculated inside a permanent half spherical drop (time-averaged shape). This is clearly the reason why EWOD-induced streaming current can be thought of as an efficient flow generator at micro-scale.

C. Numerical calculations and comparison with experiments on PBS drops in air

From the literature,[27] the streaming Reynolds number, $R_k^s = \frac{\rho (U_k^\infty)^2}{\xi_k \eta}$, depends on the oscillating mode, k = 2,4,.etc. In our case, its value is never negligibly small ($R_k^s \sim 10 - 100$, see, e.g., Table III) and consequently, the drop flow cannot be considered as creeping. Hence, numerical

TABLE III. Typical values of the parameters associated to streaming theory for water drops in air (drop volume: 1.5 μl).

Voltage frequency: $\frac{\omega_k}{2\pi}$	Mechanical frequency: $\frac{\xi_k}{2\pi}$	A_k/R_o	$\delta_s = \sqrt{\frac{\eta}{\rho\xi_k}}$	$S = \frac{\xi_k R_o}{U_k^\infty}$	$R_k^s = \frac{\rho(U_k^\infty)^2}{\eta\xi_k}$
100 Hz	200 Hz	0.3	4×10^{-5}	3.33	90
1000 Hz	2000 Hz	0.05	10^{-5}	20	25

TABLE IV. Eigenmodes and resonant frequencies for PBS drops in air (drop volume: 1.5 μl). Consider also Ref. 21 for viewing resonant drop shape oscillations.

Eigenmode k	2	4	6	8	10	12
Resonant frequency ξ_k ($\pm$10 Hz)	110	216	393	600	835	1093

simulations are conducted under Comsol® software (based on finite element method) in order to predict the drop flow induced by EWOD-streaming and to compare it with our velocimetry experiments performed with micro-PIV of fluorescent beads. The averaged drop shape considered for present calculations is supposed to be a half-sphere, which is not so restrictive since in most applications, AC EWOD delivers a contact angle close to $\pi/2$.

All the oscillating modes are time-averaged and the expression (1) for the surface velocity is introduced as a boundary condition along the drop surface for each mode considered. In this way, drop shape oscillations are nevertheless taken into account through their impact upon the tangential momentum which is injected from the Stokes layer. Due to 2-D axisymmetry, flow calculation is performed within a meridian cross-section and two slip conditions are imposed along the vertical drop axis and the underlying substrate lubricated with a thin film of RT5 oil (thickness: $\sim$260 nm (Ref. 16)).

For sake of comparison, we select experiments conducted on drops of PBS in air as ambient phase. The actuation frequency is set to values small enough to promote a standing capillary wave all along the drop surface (see Table IV for the dependence of resonant frequencies on the eigenmode k). This experimental requirement allows us to be consistent with the steady surface velocity as predicted by Eq. (1). Top and side views of the inner flow as produced under oscillating EWOD (f = 110 Hz, mode k = 2) are displayed in Figs. 3(a) and 3(b). Two (axisymmetric) toroidal vortices are (is) consistently made evident from imaging of fluorescent beads and for sake of comparison, streamlines are calculated within a meridian cross-section (Fig. 3(c)).

In order to calculate the real locations of the tracers during micro-PIV developments, use was partly made of the image mapping method proposed by Kang *et al.*,[28] corrected by considerations from Minor *et al.*[29] In this way, it was possible to take into account light ray deviations due to surface curvature and jump in refractive index across the drop surface.

As regards the micro-PIV calculation of tracers trajectories, different time scales must be considered: a first and small one, T_1, associated to the time aperture of the camera, a second one associated to trajectory fluctuations, especially within the Stokes layer, which is of the order of the inverse of the actuation frequency, $T_2 = \frac{1}{\xi_k}$ with $T_2 \gg T_1$, an intermediate one, $T3$, which is the time delay between two successive frames, and finally, a larger one, T_4, which must be selected conveniently for averaging the series of frames. The steady velocities displayed in Fig. 3 are found after averaging a series of frames over time scale T_4. The time scales T_3 and T_4 are set conveniently to get both statistically invariant velocities and a high enough spatial resolution.

Hence, a fair agreement is demonstrated and it is worthy to mention that the velocity measured by micro-PIV at the vicinity of the drop apex is of same order as the numerical prediction whatever the relative mode amplitude is: u $\simeq$ 2 mm/s for $\frac{A_{k=2}}{R_o} = 0.045$ and u $\simeq$ 6.5 mm/s for $\frac{A_{k=2}}{R_o} = 0.06$ (see Figs. 3 and 4).

A satisfying agreement between experiments on drops in air and numerical predictions is also found for oscillation modes k = 4 and 6, for which the actuation frequency, f, is never larger than 450 Hz (Fig. 4). The qualitative agreement is remarkable as regards the streamlines (see top of Fig. 4), while it is increasingly poor when comparison is made for larger and larger modes.[21] For k = 6, we think that the standing nature of the capillary wave becomes questionable since the mechanical energy of the radially inwards traveling capillary wave (TCW) becomes more predominant. Beyond the critical frequency, f = 450 Hz, it is no longer possible to observe toroidal flows, for instance those expected for the mode k = 8: the drop flow is no more found axisymmetric and steady. And when imaging the streamlines from above, counter-rotating vortices with rotation about an arbitrary axis are made evident.

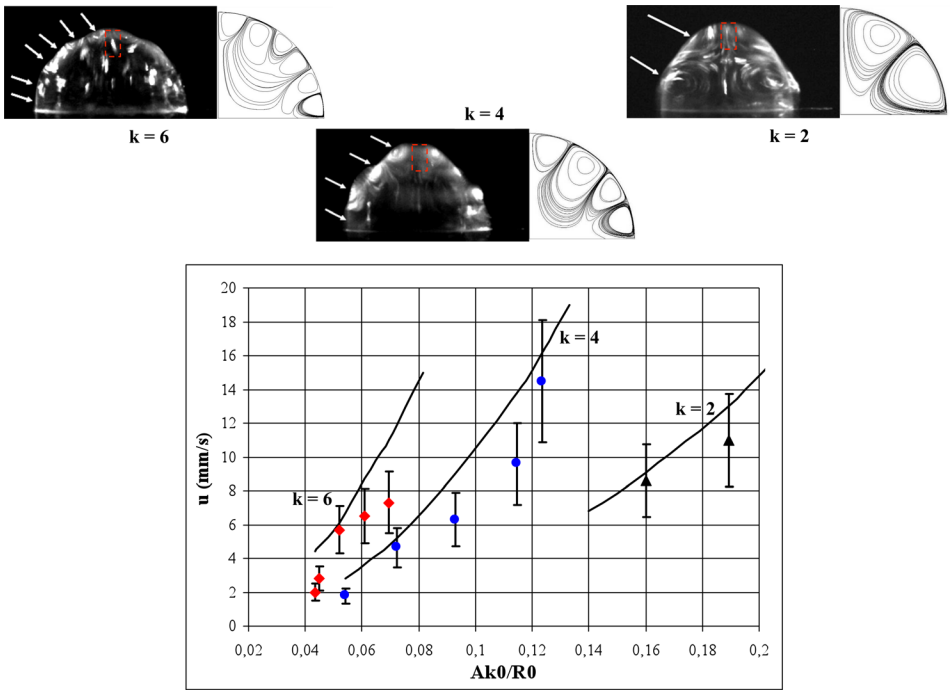

FIG. 4. Comparison (modes k = 2, 4, 6) for a sessile PBS drop in air between the velocities as measured at the apex of the drop or numerically predicted from Eq. (1) with $\theta = 0$. The experimental velocity is obtained from micro-PIV measurements especially performed on the small area bounded by the red rectangle displayed in the snapshots (tracers: fluorescent beads). The streamlines as computed numerically are made visible on the RHS of the snapshots. Chip with two half-circular electrodes separated by a gap of 3 μm, RMS voltages: 60 V (k = 2), 75 V (k = 4) or 91.7 V (k = 6). Consider also Ref. 21 for imaging of the streamlines.

D. Comments on steady internal drop flow pattern

1. Drop flows in needle electrode configuration: State of art

As already mentioned, most of the literature devoted to internal flow pattern inside a drop under EWOD focuses on the needle electrode configuration.[11,30,31] In such configuration, the meniscus motion along the needle and eventually, at least at a large enough frequency (f ∼ 10–100 KHz), the subsequent distribution of the electric potential within the drop, make the flow pattern different from the one reported in our experiences on coplanar configuration.

- Air used as ambient phase

  In the needle electrode configuration, when air is used as ambient phase, only one toroidal vortex is reported by Ko *et al.*[31] with a flow directed downwards (*upwards*) along the symmetry axis and radially outwards (*inwards*) along the supporting substrate if the actuation frequency is large enough, f ∼ 100 KHz (*small enough*, $f \sim 1$ KHz). This frequency-driven flow reversal originates from electrothermal effects.[10,32]
- Oil used as ambient phase

  Still for the needle electrode configuration, but when oil is used as ambient phase, a drop flow reversal is again found[11,30] at a small frequency (f ∼ 1 KHz at most), compared to previous experiments in air carried out by Ko *et al.*[31] at same frequency. External viscous dissipation enhanced by oil is suspected to damp the two radially inwards and outwards TCW which populate the drop surface. Since the radially inwards TCW is primarily excited from the actuated oscillating contact line, the radially outwards TCW is expected to vanish primarily under viscous damping. Therefore, remaining mechanical energy is associated to the radially inwards TCW which is suspected to explain the oil-induced flow reversal. It is worthy to recall here that Stokes drift induced by one single TCW is not the same as the one derived from a standing capillary wave.[25] This scenario seems to be confirmed by recent numerical calculations performed by Oh *et al.*[14]

2. Drop flows in coplanar electrodes configuration

Here, in our experiments on coplanar configuration, when air is used as ambient phase, the observed wave pattern has been found perfectly standing for eigenmodes k = 2, 4, 6. Both the absence of a needle as a counter-electrode and the presence of a lubricated substrate allow the apex of the drop as well as the contact line to move freely (negligible contact angle hysteresis in lubricated conditions: $<3^\circ$, see Table I). This permits the generation of a very nice standing wave all along the drop surface (provided the actuation frequency remains small enough, typically <1 KHz).

As illustrated in the following, when switching from air to oil, the drop flow pattern is again dramatically changed. But this time, in contrast to the needle configuration, here the mechanical energy of the radially inwards TCW - and related Stokes drift along the drop surface—cannot be the only reason to explain disruption of drop flow pattern.

IV. OSCILLATING EWOD IN OIL AS AMBIENT PHASE

This section is devoted to experiments in drops with biological content and silicone oil as ambient phase (viscosity: 4.9 mPa s). EWOD chip used here for biological samples is characterized by an electrode gap of 100 μm.

Consider now the shape mode equation derived by Kang *et al.*[33] with the electric stress as a source of normal momentum all along the contact line, the surface tension and the viscosity are responsible for repelling and dissipative forces, respectively.

Then, depending on the frequency of the electric actuation, it can be anticipated that the drop oscillates at different resonant modes. But due to the presence of oil outside the drop, a larger viscous dissipation of the normal component of momentum must also be expected. It is therefore consistent to check that the amplitude of drop deformation is strongly damped, especially for a large resonant frequency (eigenfrequency). Typical values of the resonant frequencies are displayed in Table V.

The surface tension between drop and oil (28 mN/m) being smaller than the one between drop and air (72 mN/m), resonant frequencies are shifted to smaller values (eigenfrequency of mode # 6: 150 Hz in oil versus 393 Hz in air). Beyond mode #10, the oscillations are no longer made evident at the apex of the drop.

At a frequency of 1 kHz and more, only the contact line oscillates, while the rest of the drop surface becomes motionless. This time, the mechanical energy of the capillary wave, excited from the contact line and traveling radially inwards to the apex of the drop, is strongly dissipated due to the significant level of the oil viscosity. As a consequence, capillary resonance at the drop apex vanishes.

As a result, the surface wave pattern is no longer standing (see Fig. 5): streaming current and subsequent stirring are mostly controlled by (damped) capillary wave traveling radially inwards from the oscillating contact line to the drop apex. This finding is consistent with previous experiments performed on needle electrode experiments with oil as ambient phase (see previous Sec. III D 1).

A. Anisotropic electrowetting and focusing of biological cells with oil as ambient phase

Experiments under oil on focusing of fluorescent beads have been presented in a companion paper.[18] Here, we present experiments conducted on biological cells and their focusing under flow. Three main results are worthy to mention:

TABLE V. Eigenmodes and resonant frequencies for PBS drops in oil (drop volume: 1.5 μl).

Eigenmode k	4	6	8	10
Resonant frequency ξ_k (± 10 Hz)	90	150	240	300

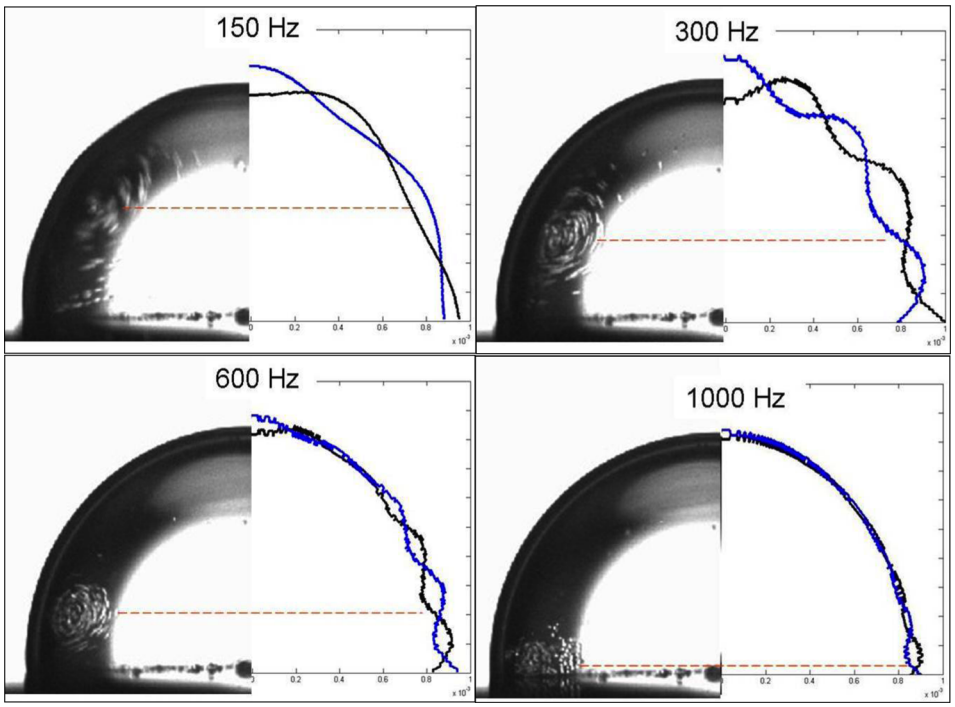

FIG. 5. Frequency-dependence of the location of U373B cell agglomerates (as imaged from the side under continuous lighting along the direction of free motion, as indicated from the horizontal dotted line) and drop shape oscillations induced by capillary waves as observed under stroboscopic lighting. For the frequencies f = (300 Hz, 600 Hz, 1 KHz), the displayed amplitude of the capillary waves is the real one multiplied by a factor 5 (better readability). Chip with two half-circular electrodes separated by a gap of 100 μm. Scaling in mm is displayed on the horizontal axis of each snapshot. RMS voltage applied: 91.7 V. Oil is used as ambient phase.

- Experiments being conducted with oil as ambient phase, the flow pattern is no more a series of axisymmetric toroidal vortices but a counter-rotating vortex pair. This can be partly explained by the fact that the radially outwards TCW is first damped under viscous dissipation. But here, in contrast with experiments under oil conducted on the needle electrode configuration,[11,30] one finds in addition a break-up of the axial symmetry so that the counter-rotating vortex pair observed differs dramatically from a vortical torus.
- By increasing the frequency of the electric voltage, the size of the vortices becomes smaller. The centrifugation and buoyancy make biological cells—except the red blood cells—to focus towards the low-pressure core of the vortices, giving rise to rotating agglomerates (Figs. 5 and 8).

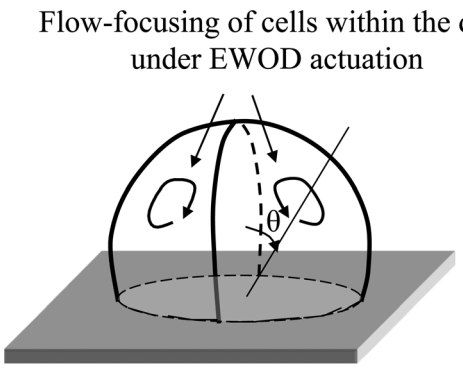

f	θ
150 hz	62°
300 hz	73°
600 hz	79°
1000 hz	86°

FIG. 6. Positioning of agglomerates as a function of the EWOD actuation frequency, as described by the angular deviation, θ (colatitude).

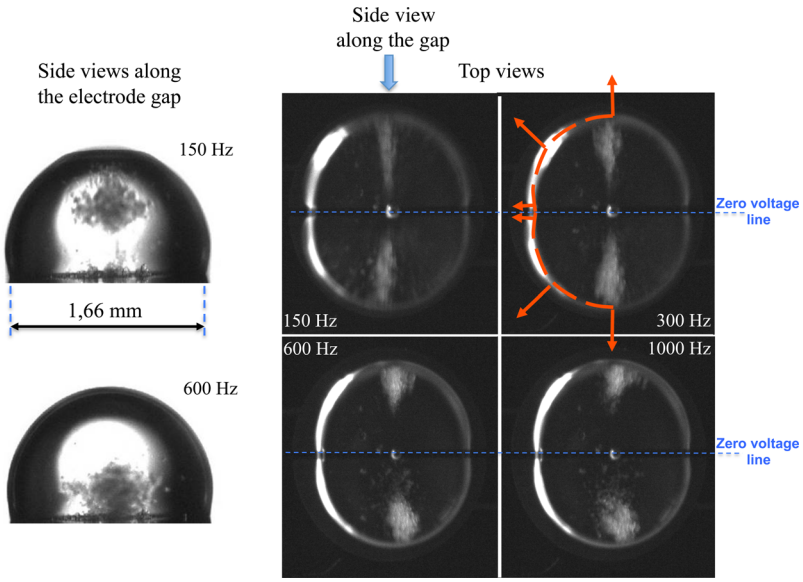

FIG. 7. Frequency-dependence of the vertical positioning of U373B cell clusters as made evident from side and top views of a drop consisting of culture medium in oil as ambient phase. Pinch-off is made evident at the location where the contact line crosses the axis of the electrode gap (top view). Chip with two half-circular electrodes separated by a gap of 100 μm. Mean wetting radii: see also Fig. 9, RMS voltage: 91.7 V.

- The positioning of the two vortices is observed to be frequency-dependent: for a frequency of electric actuation as small as 150 Hz, cell agglomerates are located at mid-height of the drop (Fig. 6) while for a higher frequency, f $\sim$ 1 KHz, they gradually get closer to the wetting plane, away from the electrode gap. Correlatively, at a large frequency, the most energetic drop deformation is confined near the contact line and therefore driven by the radially inwards traveling capillary wave.

  The monitoring of the oscillation mode being very robust, cell agglomerates can be moved precisely and reversibly by adjusting the frequency of the electric signal.

Top and side views of the actuated droplet populated by biological cells (Figs 7 and 8) reveal two significant differences in comparison with the experiments on beads:

- the side view demonstrates the presence of a counter-rotating vortex pair (two vortices only) which differs significantly from a quadripolar configuration[18] or from toroidal vortices (Fig. 3),

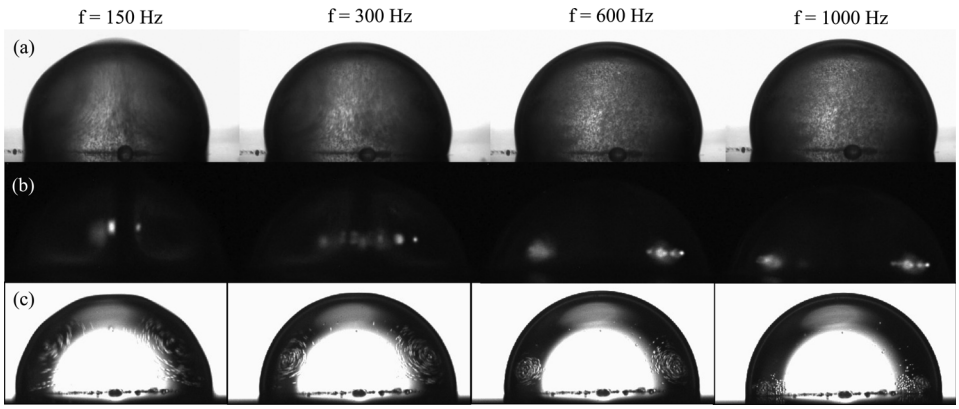

FIG. 8. Impact of drop vortical flows on different types of biological cells: (a) red blood cells, (b) white blood cells, (c) U373B cells, as demonstrated from side view along the direction of free motion (Fig. 3). Oil is used as ambient phase. Chip with two half-circular electrodes separated by a gap of 100 μm, RMS voltage: 91.7 V.

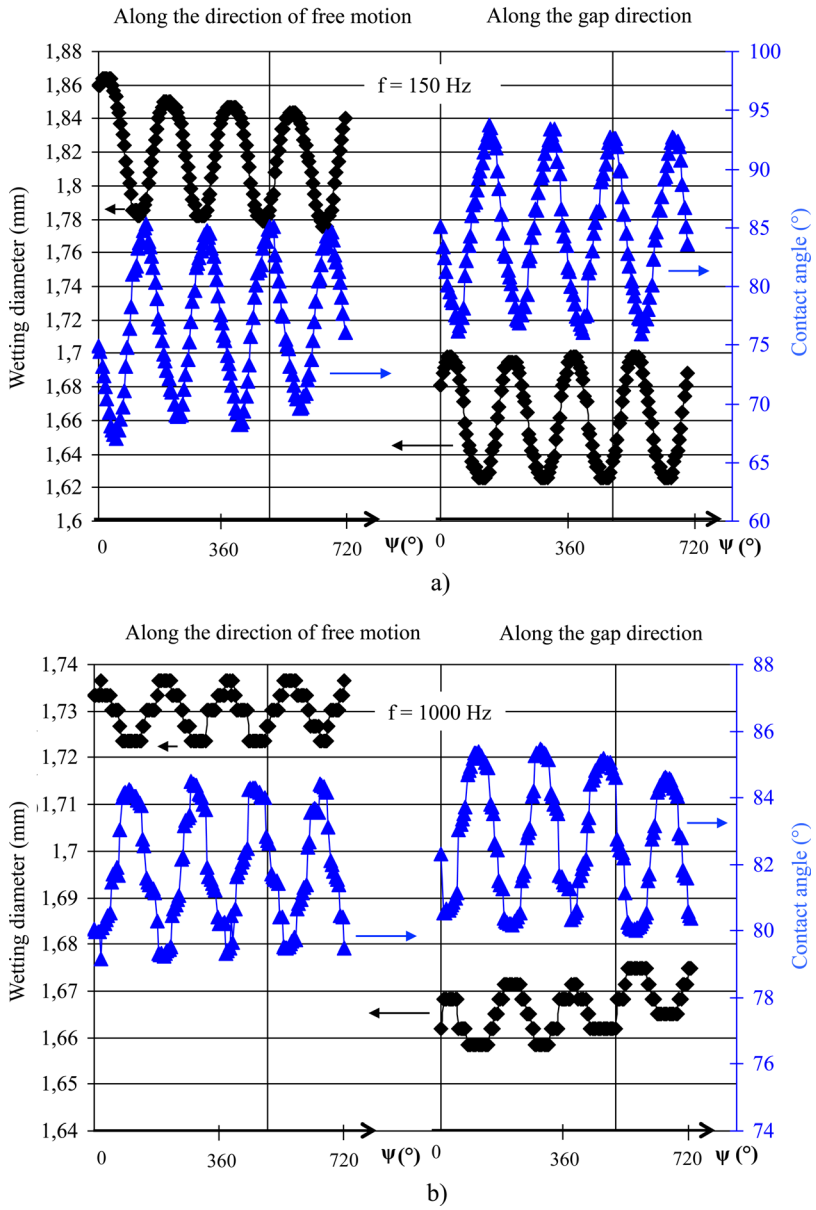

FIG. 9. Dynamics of anisotropic EWOD as characterized by oscillating wetting diameters (◆) and contact angles (▲) either along the direction of free motion (left part) or along the electrode gap (right part). The symbol, $\Psi(^\circ) = \xi_k t$, is the argument of the oscillating drop shape. The arrows connect the curves to their respective y-axis. Experimental conditions: oil is used as ambient phase; half-circular electrodes separated by a gap of 100 μm; applied RMS voltage: 91.1 V; actuation frequencies: (a) f = 150 Hz or (b) f = 1 KHz.

- top and side views (Fig. 7) demonstrate that cell clusters do not move along the surface of the drop: white blood and U373B cells remain within the bulk of the drop and move vertically down to the wetting plane.

We now focus on axial symmetry break-up of the drop flow and the monitoring of cell agglomerates.

B. Symmetry break-up of electrowetting and decisive role of the electrode gap

In a recent paper,[34] it was demonstrated that when a drop is straddling two actuated square electrodes,[35] whose transversal size (800 μm) is a little bit smaller than the drop size (~1 mm),

the contact line is able to extend up to the electrode edge under EWOD actuation. In that case, the contact line is locally trapped due to an electrically induced wetting singularity, while it remains still free to move along the length of the electrode pair. This break-up of wetting symmetry causes a fundamental change in stirring flow.

As recently demonstrated by Mampallil *et al.*,[36] wetting singularities can also be mechanically provoked by introducing on part of the hydrophobic and dielectric substrate, artificial pinning sites created by coating small gold stripes or patches of silver paste.

Here, a third scenario is made evident: we observe that the presence of an electrode gap of 100 μm and the use of silicone oil as ambient phase can also disrupt flow symmetry. As made evident by means of imaging (see top view of Fig. 7), the peanut-shaped drop is slightly pinched off at the electrode gap which causes a wetting asymmetry also demonstrated by the oscillations of the contact line and the contact angle (Fig. 9).

The amplitude of the oscillating motion of the contact line is about the same in both directions of imaging (40 μm at 150 Hz and 7 μm at 1000 Hz), but the time-averaged base radius is significantly reduced when the drop is observed along the axis of the electrode gap (differences between wetting diameters along the two directions: 160 μm at 150 Hz and 65 μm at 1000 Hz, respectively).

Symmetry break-up is also made evident from the contact angle: the averaged angle is larger when the drop is observed along the gap direction (differences in contact angles: about 9.5° at 150 Hz and 1° at 1 KHz, respectively) while amplitudes of the oscillating angle are almost kept constant. Symmetry break-up can therefore be interpreted as the result of a local reducing of the electric stress across the electrode gap, whose impact upon the contact angle is amplified by a surface tension in oil lower than the one in air (Lippman-Young equation). By considering the theory of coplanar electrowetting,[37] it is possible to demonstrate that the actuation voltage along the axis of the electrode gap is exactly zero, which means that the hydrophobic angle could be virtually recovered at the middle of the gap.

V. CONCLUDING REMARKS

In this paper, coplanar electrowetting on dielectrics (EWOD) is extensively investigated in isotropic conditions with a dedicated circular chip design. This permits to develop analytical and numerical calculations of EWOD streaming-induced drop flows which are favorably compared with experiments on PBS drops in air at a frequency never larger than 500 Hz. Then, it is demonstrated that the frequency of the applied voltage allows the end-user to monitor the flow pattern under AC EWOD.

The role of the ambient phase (air versus silicone oil) is also demonstrated to be a key parameter since both the presence of an radially inwards TCW, the presence of an electrode gap in coplanar EWOD as well as the lower value of the surface tension (aqueous drop in oil) are jointly responsible for the break-up of isotropic wetting: flow pattern switches from a series of toroidal vortices to a counter-rotating vortex pair.

Drop flows in oil exhibit interesting features especially relevant to situations when biological cells are used. Agglomerates of cells are created from the presence of a counter-rotating vortex pair. They move towards the wetting plane under the effect of the viscous damping of capillary waves at a high enough frequency of the applied AC voltage. This displacement is found quite reversible and reproducible when use is made of the voltage frequency as a monitoring parameter.

The reason why the cells concentrate in the drop volume rather than at the surface is probably related to their mass density which, though it has not been measured, is expected to be different from the mass density of the fluorescent beads ($\rho = 1.05$). Further investigation should be continued in particular in order to understand why focusing effect is less marked with red blood cells than with white blood or U373B cells. The respective influences of surface rheology between the drop and the ambient phase, of the mass density of cells, of their volume concentration, of the shape or deformability of cells as well, should be studied extensively thereafter.

To conclude, it is conceivable to exploit the EWOD-induced focusing in order to concentrate or manipulate biological entities in digital lab-on-a-chips. One application might be to facilitate antibody-antigens interactions within microdrops. For instance, adsorption of DNA strands on functionalized beads could be facilitated if DNA strands and corresponding beads are concentrated within the core of the same vortex or if one of them is grafted onto the substrate (a high frequency should be selected).

From this study, new design guidelines on EWOD-based lab-on-a-chips and their frequency monitoring can be formulated. Specific applications can be addressed such as concentration of biological material, functionalization of solid spots,[38] mixing,[7] etc.

ACKNOWLEDGMENTS

The authors are grateful to Frederique Mittler, Myriam Cubizolles and Fabrice Navarro, from CEA-LETI-DTBS, for their decisive help in the handling of biological cells. The authors would like to thank reviewer #1 for helpful comments on drop flows in the needle electrode configuration.

[1]S. Ko, S. Lee, and K. Kang, Appl. Phys. Lett. **94**, 194102 (2009).
[2]V. Hessel, H. Lowe, and F. Schonfeld, Chem. Eng. Sci. **60**, 2479 (2005).
[3]B. Berge and J. Peseux, Eur. Phys. J. E **3**, 159 (2000).
[4]R. Hayes and B. Feenstra, Nature **425**, 383 (2003).
[5]M. G. Pollack, V. K. Pamula, V. Srinivasan, and A. E. Eckhardt, Expert Rev. Mol. Diagn. **11**, 393 (2011).
[6]C. Delattre, C. P. Allier, Y. Fouillet, D. Jary, F. Bottausci, D. Bouvier, G. Delapierre, M. Quinaud, A. Rival, L. Davoust, and C. Peponnet, Biosens. Bioelectron. **36**, 230 (2012).
[7]R. Malk, A. Rival, Y. Fouillet, and L. Davoust, ASME Conf. Proc. **2010**, 239.
[8]C.-P. Lee, H.-C. Chen, and M.-F. Lai, Biomicrofluidics **6**, 012814 (2012).
[9]R. Miraghaie, J. Sterling, and A. Nadim, NSTI-Nanotech. **2**, 610 (2006).
[10]H. Lee, S. Yun, S. Ko, and K. Kang, Biomicrofluidics **3**, 044113 (2009).
[11]F. Mugele, A. Staicu, R. Bakker, and D. van den Ende, Lab Chip **11**, 2011 (2011).
[12]A sessile drop stays on a dielectric film with a first electrode underneath and a needle electrode above which is put in capillary contact with drop apex.
[13]R. Malk, *Ecoulements en gouttes activés par électromouillage*, Ph.D. thesis, Université de Grenoble (2011).
[14]J. Oh, D. Legendre, and F. Mugele, EPL **98**, 34003 (2012).
[15]C. Picard and L. Davoust, Langmuir **23**, 1394 (2007).
[16]J. Theisen and L. Davoust, Langmuir **28**, 1041 (2012).
[17]L. Davoust and J. Theisen, "Evaporation rate of drop arrays within a digital microfluidic system," Sensors Actuators B (in press).
[18]R. Malk, Y. Fouillet, and L. Davoust, Sensors Actuators B **154**, 191 (2011).
[19]U373B cells are nothing but modified astrocytes commonly used as a control means to identify the cytotoxicity of certain components.
[20]J. R. Saylor, A. J. Szeri, and G. P. Foulks, Exp. Fluids **29**, 509 (2000).
[21]See supplementary material at http://dx.doi.org/10.1063/1.4817006 for viewing resonant drop shape oscillations under stroboscopic lighting and for imaging of the streamlines.
[22]J. M. Oh, S. Ko, and K. Kang, Langmuir **24**(15), 8379 (2008).
[23]H. Lamb, *Hydrodynamics* (Cambridge University Press, 1932).
[24]J. B. Bostwick and P. H. Steen, Phys. Fluids **21**, 032108 (2009).
[25]G. Batchelor, *Introduction to Fluid Mechanics* (Cambridge University Press, 2000).
[26]H. Schlichting and K. Gersten, *Boundary-Layer Theory* (Springer, 1979).
[27]J. Stuart, J. Fluid Mech. **87**, 624 (1966).
[28]K. Kang, S. J. Lee, C. Lee, and I. S. Kang, Meas. Sci. Technol. **15**, 1104 (2004).
[29]G. Minor, P. Oshkai, and N. Djilali, Meas. Sci. Technol. **18**, L23 (2007).
[30]F. Mugele, J.-C. Baret, and D. Steinhauser, Appl. Phys. Lett. **88**, 204106 (2006).
[31]S. Ko, H. Lee, and K. Kang, Langmuir **24**, 1094 (2008).
[32]P. Garcia-Sanchez, A. Ramos, and F. Mugele, Phys. Rev. E **81**, 015303 (2010).
[33]J. M. Oh, S. H. Ko, and K. H. Kang, Phys. Fluids **22**, 032002 (2010).
[34]R. Malk, J. Theisen, Y. Fouillet, and L. Davoust, Microelectron. Eng. **97**, 306 (2012).
[35]Common geometry involved in EWOD-based lab-on-a-chips.
[36]D. Mampallil, D. van den Ende, and F. Mugele, Appl. Phys. Lett. **99**, 154102 (2011).
[37]U.-C. Yi and C.-J. Kim, Micromech. Microeng. **16**, 2053 (2006).
[38]R. Malk, Y. Fouillet, and L. Davoust, Microelectron. Eng. **88**, 1745 (2011).